


Can the state $Y(4626)$ be a P -wave tetraquark state $[cs][\bar{c}\bar{s}]$?

Chengrong Deng^{1,*}, Hong Chen^{1,†} and Jialun Ping^{2,‡}

¹*Department of Physics, Southwest University, Chongqing 400715, China*

²*Department of Physics, Nanjing Normal University, Nanjing 210097, China*

 (Received 16 December 2019; accepted 12 March 2020; published 30 March 2020)

Stimulated by the state $Y(4626)$ recently reported by the Belle Collaboration, we utilize a multi-quark color flux-tube model with a multibody confinement potential and one-gluon-exchange interaction to make an exhaustive investigation on the diquark-antidiquark state $[cs][\bar{c}\bar{s}]$. Numerical results indicate that the spatial configuration of the states $[cs][\bar{c}\bar{s}]$ like a dumbbell, the larger the orbital excitation L , the farther the distance between the diquark $[cs]$ and the antidiquark $[\bar{c}\bar{s}]$, the more clearer the shape. The mixing of the color configurations $[[cs]_{\bar{3}_c}[\bar{c}\bar{s}]_{\bar{3}_c}]_1$ and $[[cs]_{6_c}[\bar{c}\bar{s}]_{\bar{6}_c}]_1$ in the ground states is strong, while the color configuration $[[cs]_{\bar{3}_c}[\bar{c}\bar{s}]_{\bar{3}_c}]_1$ is absolutely predominant in the excited states. The states $Y(4626)$, $Y(4630)$, and $Y(4660)$ can be uniformly described as the P -wave tetraquark state $[cs][\bar{c}\bar{s}]$ with 1^{--} . The states $Y(4626)$ and $Y(4630)$ can be described as the same state consisting of a scalar $[cs]$ and a scalar $[\bar{c}\bar{s}]$, while the state $Y(4660)$ is made of a scalar $[cs]$ ($[\bar{c}\bar{s}]$) and an axial-vector $[\bar{c}\bar{s}]$ ($[cs]$). Their hidden-bottom partner is predicted in the model calculation. The states $X(4140)$, $X(4274)$, $X(4350)$, $X(4500)$, and $X(4700)$ are also discussed.

DOI: 10.1103/PhysRevD.101.054039

I. INTRODUCTION

The past decade or so has witnessed the great prosperity of the development of hadron physics. A large number of hidden charmed and bottomed hadrons were subsequently observed in experiments [1], some of which, such as charged states Z_b and Z_c , are difficult to accommodate in the naive quark model. Very recently, the Belle Collaboration reported a vector charmoniumlike state in the process of $e^+e^- \rightarrow D_s^+ D_{s1}(2536)^- + c.c.$ via initial-state radiation [2]. The state has respectively a measured mass and width of $4265.9_{-6.0}^{+6.2} \pm 0.4$ MeV and $49.8_{-11.5}^{+13.9} \pm 4.0$ MeV and decays into a charmed anti-strange and anticharmed-strange meson pair $D_s^+ D_{s1}(2536)^-$ with a significance of 5.9σ , which are consistent with those of the states $Y(4630)$ and $Y(4660)$ within errors although they are observed in the different processes [3,4]. The state is suggested as an exotic charmoniumlike state with 1^{--} , called $Y(4626)$ [2], which provides an ideal opportunity to research the low-energy strong interaction. The most intuitive information provided by the decay behavior of

the state $Y(4626)$ is that its main component is likely to be a tetraquark system $cs\bar{c}\bar{s}$.

In analogy with the deuteron, which is bound through the exchange of pion and other light mesons [5], Karliner and Rosner predicted the masses of tetraquark state $cs\bar{c}\bar{s}$ based on the proximity to thresholds of $D_s\bar{D}_s$ pairs [6]. Albuquerque and Nielsen described the state $Y(4660)$ as the state $[cs][\bar{c}\bar{s}]$ with QCD sum rules [7]. Inspired by the states $X(4140)$, $X(4274)$, $X(4500)$, $X(4700)$, and $Y(4140)$, the tetraquark state $cs\bar{c}\bar{s}$ was also systematically researched in various theoretical frameworks, such as simple color-magnetic interaction models [8,9], the QCD sum rule [10–12], nonrelativistic and relativistic quark models [13,14], the diquark model [15], and lattice QCD [16]. A question then arises as to whether or not the main component of the states $Y(4626)$ can be described as the tetraquark state $[cs][\bar{c}\bar{s}]$. Therefore, chiral constituent quark model and quasipotential Bethe-Salpeter equation with the one-boson-exchange model were immediately used to describe the state $Y(4626)$ as a molecular state of $D_s^* \bar{D}_{s1}(2536)$ with 1^{--} [17].

A multi-quark color flux-tube model based on the lattice QCD picture and the traditional quark models has been developed to study multi-quark states, in which the multibody confinement potential is a dynamical mechanism in the formation and decay of the multi-quark states [18]. Similar multibody string models were also extensively applied to study the properties of multi-quark states [19,20]. In this work, we move on to the investigation on the tetraquark state $[cs][\bar{c}\bar{s}]$ to interpret the inner

*crdeng@swu.edu.cn

†chenh@swu.edu.cn

‡jlping@njnu.edu.cn

Published by the American Physical Society under the terms of the *Creative Commons Attribution 4.0 International license*. Further distribution of this work must maintain attribution to the author(s) and the published article's title, journal citation, and DOI. Funded by SCOAP³.

structures of the states $Y(4626)$, $Y(4630)$, and $Y(4660)$ within the framework of the multiquark color flux-tube model, which is anticipated to exhibit new insights into the binding mechanisms in multiquark states, and maybe improve understanding of QCD in the nonperturbative regime.

This paper is organized as follows. After the Introduction section, the presentation of the multiquark color flux-tube model is given in Sec. II. The wave function of the tetraquark state $[cs][\bar{c}\bar{s}]$ is shown in Sec. III. The numerical results and discussions are presented in Sec. IV. A brief summary is listed in the last section.

II. MULTIQUARK COLOR FLUX-TUBE MODEL

Constituent quark models (CQM) are formulated under the assumption that hadrons are color-singlet nonrelativistic bound states of constituent quarks with phenomenological effective masses and interactions. One expects the dynamics of the CQM to be governed by QCD. The perturbative effect is well-known one-gluon-exchange (OGE) interaction. The central part of the OGE interaction takes its form used extensively and is listed in [21]

$$V_{ij}^G = \frac{\alpha_s}{4} \lambda_i^c \cdot \lambda_j^c \left(\frac{1}{r_{ij}} - \frac{2\pi\delta(\mathbf{r}_{ij})\sigma_i \cdot \sigma_j}{3m_i m_j} \right),$$

where λ^c and σ respectively represent the Gell-Mann matrices and the Pauli matrices. The color-magnetic mechanism, which is proportional to the factor $\lambda_i^c \cdot \lambda_j^c \sigma_i \cdot \sigma_j$, in the OGE interaction leads to mass splitting among different color-spin configurations. α_s is a running strong coupling constant in the perturbative QCD [22],

$$\alpha_s(\mu^2) = \frac{1}{\beta_0 \ln \frac{\mu^2}{\Lambda^2}}. \quad (1)$$

In this work, we take the form

$$\alpha_s(\mu_{ij}^2) = \frac{\alpha_0}{\ln \frac{\mu_{ij}^2}{\Lambda_0^2}}, \quad (2)$$

where μ_{ij} is the reduced mass of two interacting particles. The function $\delta(\mathbf{r}_{ij})$ should be regularized [23],

$$\delta(\mathbf{r}_{ij}) = \frac{1}{4\pi r_{ij} r_0^2(\mu_{ij})} e^{-r_{ij}/r_0(\mu_{ij})}, \quad (3)$$

where $r_0(\mu_{ij}) = \hat{r}_0/\mu_{ij}$. Λ_0 , α_0 , μ_0 , and \hat{r}_0 are adjustable model parameters determined by fitting the data of $q\bar{q}$ -mesons.

Color confinement is one of the most prominent features of QCD and should play an essential role in the low-energy hadron physics. At present, it is still impossible for us to derive color confinement analytically from the QCD

Lagrangian. Color confinement is a long-distance behavior whose understanding continues to be a challenge in theoretical physics. The color confinement potential in the traditional constituent quark model can be phenomenologically described as the sum of two-body interactions proportional to the color charges and r_{ij}^2 [24],

$$V^C = -a_c \sum_{i>j}^n \lambda_i^c \cdot \lambda_j^c r_{ij}^2, \quad (4)$$

where r_{ij} is the distance between two interacting quarks q_i and q_j . The model can automatically prevent overall color-singlet multiquark states disintegrating into several color subsystems by means of color confinement with an appropriate $SU_c(3)$ Casimir constant [25]. In contrast, the model allows a multiquark system dissociating into color-singlet clusters, and it leads to interacting potentials within mesonlike $q\bar{q}$ and baryonlike qqq subsystems in accord with the empirically known potentials [25]. However, the model is known to be flawed phenomenologically because it leads to power law van der Waals forces between color-singlet hadrons. In addition, it also leads to anticonfinement for symmetrical color structure in the multiquark system [26].

Up to now, color confinement can be established both from gauge-invariant lattice QCD (LQCD) simulations and from experimental observations like Regge trajectories [27,28]. $q\bar{q}$ systems can be well reproduced at short distances by a linear potential. Such a potential can be physically interpreted in a picture in which the quark and the antiquark are linked with a three-dimensional color flux tube. In the dual superconductor picture of color confinement [29], the color flux tube is formed due to the dual Meissner effect caused by monopole condensation. The chromoelectric field lines between color sources, like a quark and antiquark pair, are squeezed into a narrow flux tube along the line connecting the pair. Color flux tubes play significant roles in many interesting places of hadron physics, such as color confinement, quark pair creation, and hadron structure.

LQCD calculations on baryons, tetraquark, and pentaquark states revealed that there exist flux-tube structures [30]. In the case of a given spatial configuration of multiquark states, the confinement is a multibody interaction and can be simulated by a static potential, which is proportional to the minimum of the total length of color flux tubes. A naive flux-tube model, used in the present work, based on this picture has been constructed [18]. It takes into account multibody confinement with harmonic interaction approximation, i.e., where the length of the color flux tube is replaced by the square of the length to simplify the numerical calculation. There are two theoretical arguments to support this approximation. One is that the spatial separations of the quarks (lengths of the color flux

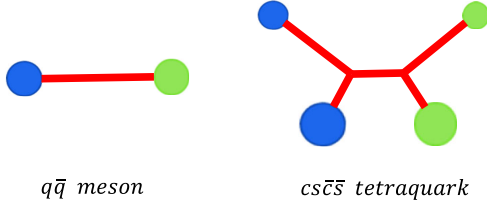


FIG. 1. Color flux-tube structures.

tube) in hadrons are not large, so the difference between the linear and quadratic forms is small and can be absorbed in the adjustable parameter, the stiffness. The other is that we are using a nonrelativistic description of the dynamics, and, as was shown long ago [31], an interaction energy that varies linearly with separation between fermions in a relativistic, first-order differential dynamics has a wide region in which a harmonic approximation is valid for the second-order (Feynman-Gell-Mann) reduction of the equations of motion. We calculated the $b\bar{b}$ spectrum by using quadratic and linear potentials, the results showing that the differences between two potentials are small for the low-lying states [32]. In addition, the calculations on nucleon-nucleon interactions also support the replacement [33].

The color flux-tube structures of $q\bar{q}$ -mesons and the tetraquark state $[cs][\bar{c}\bar{s}]$ with diquark-antidiquark configuration are shown in Fig. 1, in which the blue and green disks, respectively, represent the quark and antiquark. In the tetraquark state $[cs][\bar{c}\bar{s}]$, the big disk stands for a heavy quark, while the small one stands for a light quark. The quark and antiquark in the mesons are linked with a three-dimensional color flux tube. A two-body confinement potential can be written as

$$V_{\min}^C(2) = Kr^2, \quad (5)$$

where r is the distance between the quark and antiquark and the parameter K is the stiffnesses of a three-dimensional color flux-tube and determined by fitting the ground heavy-meson spectra. In the state $[cs][\bar{c}\bar{s}]$, the codes of the quarks (antiquarks) c , s , \bar{c} , and \bar{s} are assumed to be 1, 2, 3, and 4, respectively. According to a double Y-shaped color flux-tube structure of the state $[cs][\bar{c}\bar{s}]$, a four-body quadratic confinement potential instead of linear one used in the LQCD can be written as

$$V^C(4) = K[(\mathbf{r}_1 - \mathbf{y}_{12})^2 + (\mathbf{r}_2 - \mathbf{y}_{12})^2 + (\mathbf{r}_3 - \mathbf{y}_{34})^2 + (\mathbf{r}_4 - \mathbf{y}_{34})^2 + \kappa_d(\mathbf{y}_{12} - \mathbf{y}_{34})^2], \quad (6)$$

in which \mathbf{r}_1 , \mathbf{r}_2 , \mathbf{r}_3 , and \mathbf{r}_4 , respectively, represent the position of the corresponding quark (antiquark). Two Y-shaped junctions \mathbf{y}_{12} and \mathbf{y}_{34} are variational parameters, which can be determined by taking the minimum of the confinement potential. The relative stiffness parameter κ_d is equal to $\frac{C_d}{C_3}$ [34], where C_d is the eigenvalue of the Casimir

operator associated with the $SU(3)$ color representation d at either end of the color flux tube, such as $C_3 = \frac{4}{3}$, $C_6 = \frac{10}{3}$, and $C_8 = 3$.

The minimum of the confinement potential $V_{\min}^C(4)$ can be obtained by taking the variation of $V^C(4)$ with respect to \mathbf{y}_{12} and \mathbf{y}_{34} , and it can be expressed as

$$V_{\min}^C(4) = K \left(\mathbf{R}_1^2 + \mathbf{R}_2^2 + \frac{\kappa_d}{1 + \kappa_d} \mathbf{R}_3^2 \right). \quad (7)$$

The canonical coordinates \mathbf{R}_i have the following forms:

$$\begin{aligned} \mathbf{R}_1 &= \frac{1}{\sqrt{2}}(\mathbf{r}_1 - \mathbf{r}_2), & \mathbf{R}_2 &= \frac{1}{\sqrt{2}}(\mathbf{r}_3 - \mathbf{r}_4), \\ \mathbf{R}_3 &= \frac{1}{\sqrt{4}}(\mathbf{r}_1 + \mathbf{r}_2 - \mathbf{r}_3 - \mathbf{r}_4), \\ \mathbf{R}_4 &= \frac{1}{\sqrt{4}}(\mathbf{r}_1 + \mathbf{r}_2 + \mathbf{r}_3 + \mathbf{r}_4). \end{aligned} \quad (8)$$

The use of $V_{\min}^C(n)$ can be understood here as that the gluon field readjusts immediately to its minimal configuration.

The diquark $[cs]$ and antidiquark $[\bar{c}\bar{s}]$ can be considered as compound bosons \bar{Q} and Q with no internal orbital excitation, and the orbital excitation \mathbf{L} is assumed to occur only between Q and \bar{Q} in the present work. To facilitate numerical calculations, the spin-orbit interactions are assumed to take place approximately between compound bosons \bar{Q} and Q , which is consistent with the work [35]. The spin orbit-related interactions can be expressed as

$$V_{\bar{Q}Q}^{G,LS} \approx \frac{\alpha_s}{4} \lambda_{\bar{Q}}^{\bar{c}} \cdot \lambda_Q^c \frac{1}{8M_{\bar{Q}}M_Q} \frac{3}{X^3} \mathbf{L} \cdot \mathbf{S}, \quad (9)$$

$$V_{\bar{Q}Q}^{C,LS} \approx \frac{K}{4M_{\bar{Q}}M_Q} \frac{\kappa_d}{1 + \kappa_d} \mathbf{L} \cdot \mathbf{S}, \quad (10)$$

where the masses of the compound bosons $M_Q = M_{\bar{Q}} \approx m_c + m_s$, X is the distance between the two compound bosons, and S stands for the total spin angular momentum of the state $[cs][\bar{c}\bar{s}]$.

The complete Hamiltonian involving the multibody confinement potential and OGE interaction for the heavy mesons and the states $[cs][\bar{c}\bar{s}]$ can be presented as

$$\begin{aligned} H_n &= \sum_{i=1}^n \left(m_i + \frac{\mathbf{p}_i^2}{2m_i} \right) - T_C + \sum_{i>j}^n (V_{ij}^G + V_{ij}^{G,LS}) \\ &+ V_{\min}^C(n) + V_{\min}^{C,LS}(n). \end{aligned} \quad (11)$$

T_C is the center-of-mass kinetic energy of the state and should be deducted; \mathbf{p}_i is the momentum of the i th quark (antiquark). LQCD computations on the static tetraquark potential show that the tetraquark potential is consistent

with a four-body confining potential plus one-gluon-exchange Coulomb potentials [36].

It is worth mentioning that the multi-quark color flux-tube model is not a completely new model but the updated version of the traditional CQM based on the color flux-tube picture of hadrons in the LQCD. In fact, it merely modifies the two-body confinement potential in the traditional CQM into the multibody one to describe multi-quark states with multibody interaction. Furthermore, the multi-quark color flux-tube model can overcome the disadvantages of the traditional CQM.

III. WAVE FUNCTION OF THE STATE $[cs][\bar{c}\bar{s}]$

The numerical results of the state $[cs][\bar{c}\bar{s}]$ should be solved using a complete wave function which includes all possible flavor-spin-color-spatial channels that contribute to a given well-defined parity, isospin, and total angular momentum. Within the framework of the diquark-antidiquark configuration, the wave function of the state $[cs][\bar{c}\bar{s}]$ can be constructed as a sum of the following direct products of color χ_c , isospin η_i , spin χ_s , and spatial ϕ_{lm}^G terms:

$$\begin{aligned} \Phi_{IM_J JM_J}^{[cs][\bar{c}\bar{s}]} &= \sum_{\alpha} \xi_{\alpha} [[\phi_{l_a m_a}^G(\mathbf{r}) \chi_{s_a}^{[cs]}]_{s_a}^{[cs]} \phi_{l_b m_b}^G(\mathbf{R}) \\ &\times \chi_{s_b}^{[\bar{c}\bar{s}]}]_S^{[\bar{c}\bar{s}]} \phi_{LM}^G(\mathbf{X})]_{JM_J}^{[cs][\bar{c}\bar{s}]} \\ &\times [\eta_{i_a}^{[cs]} \eta_{i_b}^{[\bar{c}\bar{s}]}]_{IM_I}^{[cs][\bar{c}\bar{s}]} [\chi_{c_a}^{[cs]} \chi_{c_b}^{[\bar{c}\bar{s}]}]_{CW_C}^{[cs][\bar{c}\bar{s}]} . \end{aligned} \quad (12)$$

The subscripts a and b in the intermediate quantum numbers represent the diquark $[cs]$ and antidiquark $[\bar{c}\bar{s}]$, respectively. The summing index α stands for all possible flavor-spin-color-spatial intermediate quantum numbers. The parity of the state $[cs][\bar{c}\bar{s}]$ is related to the orbital excitations \mathbf{L} as $P = (-1)^L$ because of $l_a = 0$ and $l_b = 0$. Considering a pair of charge-conjugated bosons $Q\bar{Q}$, we can obtain the C -parity $C = (-1)^{L+S-s_a-s_b}$ because the total wave function has to be completely symmetric under exchange of coordinates and spin of the bosons Q and \bar{Q} .

The relative spatial coordinates \mathbf{r} , \mathbf{R} , and \mathbf{X} in the state $[cs][\bar{c}\bar{s}]$ can be defined as

$$\begin{aligned} \mathbf{r} &= \mathbf{r}_1 - \mathbf{r}_2, & \mathbf{R} &= \mathbf{r}_3 - \mathbf{r}_4 \\ \mathbf{X} &= \frac{m_1 \mathbf{r}_1 + m_2 \mathbf{r}_2}{m_1 + m_2} - \frac{m_3 \mathbf{r}_3 + m_4 \mathbf{r}_4}{m_3 + m_4} . \end{aligned}$$

In the dynamical calculation, the relative motion wave functions $\phi_{l_a m_a}^G(\mathbf{r})$, $\phi_{l_b m_b}^G(\mathbf{R})$, and $\phi_{LM}^G(\mathbf{X})$ can be expressed as the superposition of many different-size Gaussian functions with well-defined quantum numbers, which share the exact same form with Eq. (15) in Sec. IV, to obtain accurate numerical results. For the sake of saving space, the explicit expressions of $\phi_{l_a m_a}^G(\mathbf{r})$, $\phi_{l_b m_b}^G(\mathbf{R})$, and $\phi_{LM}^G(\mathbf{X})$ are not

presented here. It is worth mentioning that we do not make any approximation or simplification in the course of numerical calculation in spite of a heavy computational workload.

The color representation of the diquark $[cs]$ maybe antisymmetrical $\bar{\mathbf{3}}_c$ or symmetrical $\mathbf{6}_c$, whereas that of the antidiquark $[\bar{c}\bar{s}]$ maybe antisymmetrical $\mathbf{3}_c$ or symmetrical $\bar{\mathbf{6}}_c$. Coupling the diquark and the antidiquark into an overall color singlet only have two ways: $[[cs]_{\bar{\mathbf{3}}_c} \otimes [\bar{c}\bar{s}]_{\mathbf{3}_c}]_{\mathbf{1}}$ and $[[cs]_{\mathbf{6}_c} \otimes [\bar{c}\bar{s}]_{\bar{\mathbf{6}}_c}]_{\mathbf{1}}$ according to the color coupling rule. The spin of the diquark $[cs]$ is coupled to s_a , and that of the antidiquark $[\bar{c}\bar{s}]$ is coupled to s_b . The total spin wave function of the state $[cs][\bar{c}\bar{s}]$ can be written as $S = s_a \oplus s_b$. Then, we have the following basis vectors as a function of the total spin S :

$$S = \begin{cases} 0, & 1 \oplus 1 \quad \text{or} \quad 0 \oplus 0 \\ 1, & 1 \oplus 1, 1 \oplus 0 \quad \text{or} \quad 0 \oplus 1 . \\ 2, & 1 \oplus 1 \end{cases} \quad (13)$$

For $S = 0$ and 2 , the state $[cs][\bar{c}\bar{s}]$ should have definite C -parity $(-1)^L$ because both the diquark and the antidiquark have the same spin. For $S = 1$, the C parity of the channel $1 \oplus 1$ is $(-1)^{L+1}$, while that of the channels $0 \oplus 1$ and $1 \oplus 0$ are $(-1)^L$.

The quarks c and s have isospin zero so that they do not contribute to the total isospin. The possible color-flavor-spin functions of the states $[cs][\bar{c}\bar{s}]$ with total spin S can be written as

$$S = \begin{cases} 0, & [[cs]_{\bar{\mathbf{3}}_c}^{0,1} [\bar{c}\bar{s}]_{\mathbf{3}_c}^{0,1}]_{\mathbf{1}_c}^0, [[cs]_{\mathbf{6}_c}^{0,1} [\bar{c}\bar{s}]_{\bar{\mathbf{6}}_c}^{0,1}]_{\mathbf{1}_c}^0 \\ 1, & [[cs]_{\bar{\mathbf{3}}_c}^{0,1} [\bar{c}\bar{s}]_{\mathbf{3}_c}^{0,1}]_{\mathbf{1}_c}^1, [[cs]_{\mathbf{6}_c}^{0,1} [\bar{c}\bar{s}]_{\bar{\mathbf{6}}_c}^{0,1}]_{\mathbf{1}_c}^1 , \\ 2, & [[cs]_{\bar{\mathbf{3}}_c}^1 [\bar{c}\bar{s}]_{\mathbf{3}_c}^1]_{\mathbf{1}_c}^2, [[cs]_{\mathbf{6}_c}^1 [\bar{c}\bar{s}]_{\bar{\mathbf{6}}_c}^1]_{\mathbf{1}_c}^2 \end{cases} \quad (14)$$

where the superscript and subscript denote the spin and color representations, respectively. The number of the wave functions is big because the Pauli principle is out of operation in the state $[cs][\bar{c}\bar{s}]$.

IV. NUMERICAL CALCULATIONS AND ANALYSIS

The starting point of the study on the state $[cs][\bar{c}\bar{s}]$ is to accommodate $q\bar{q}$ -mesons in the multi-quark color flux-tube model to determine model parameters. To avoid the misjudgment of the behavior of model dynamics due to inaccurate numerical results, a high-precision numerical method is therefore indispensable. The Gaussian expansion method (GEM) [37], which has been proven to be rather powerful to solve few-body problem in nuclear physics, is therefore widely used to study few-body systems. According to the GEM, the two-body relative motion wave function of $q\bar{q}$ -mesons can be written as

TABLE I. Model parameters, quark mass, and Λ_0 unit in MeV, a_c unit in $\text{MeV} \cdot \text{fm}^{-2}$, r_0 unit in $\text{MeV} \cdot \text{fm}$, and α_0 is dimensionless.

Para.	$m_{u,d}$	m_s	m_c	m_b	K	α_0	Λ_0	r_0
Valu.	313	494	1664	5006	800	4.25	40.85	119.3

TABLE II. Ground heavy-meson spectra, unit in MeV.

States	D^\pm	D^*	D_s^\pm	D_s^*	η_c	J/Ψ	B^0
Theo.	1886	2000	1982	2109	2965	3103	5261
PDG.	1869	2007	1969	2112	2980	3097	5280

States	B^*	B_s^0	B_s^*	B_c	B_c^*	η_b	$\Upsilon(1S)$
Theo.	5305	5346	5399	6244	6366	9376	9486
PDG.	5325	5366	5416	6277	...	9391	9460

$$\phi_{lm}^G(\mathbf{r}) = \sum_{n=1}^{n_{\max}} c_n N_{nl} r^l e^{-\nu_n r^2} Y_{lm}(\hat{\mathbf{r}}), \quad (15)$$

where $\mathbf{r} = \mathbf{r}_q - \mathbf{r}_{\bar{q}}$. Gaussian size parameters are taken as geometric progression

$$\nu_n = \frac{1}{r_n^2}, \quad r_n = r_1 a^{n-1}, \quad a = \left(\frac{r_{n_{\max}}}{r_1} \right)^{\frac{1}{n_{\max}-1}}. \quad (16)$$

The coefficient c_n is determined by the dynamics of systems. With $r_1 = 0.3$ fm, $r_{n_{\max}} = 2.0$ fm, and $n_{\max} = 7$, the converged numerical results can be arrived at.

The mass of the ud quark is taken to be one-third of that of the nucleon, and other adjustable model parameters in Table I can be determined by approximately strictly solving

the two-body Schrödinger equation to fit the masses of the ground states of heavy mesons in Table II.

The mass spectrum of the states $[cs][\bar{c}\bar{s}]$ with J^{PC} under the assumption of the total spin $S = 0, 1$, and 2 and orbital excitation $L = 0, 1$, and 2 in the multiquark color flux-tube model can be obtained by solving the four-body Schrödinger equation with the well-defined trial wave functions of the state $[cs][\bar{c}\bar{s}]$ involving all possible channels,

$$(H_4 - E_4)\Phi_{IM_i J M_j}^{[cs][\bar{c}\bar{s}]} = 0, \quad (17)$$

which are listed in Table III. Using the wave function of the state $[cs][\bar{c}\bar{s}]$ obtained by solving the Schrödinger equation, the mass and proportion of the color configurations $[[cs]_{\bar{3}_c}[\bar{c}\bar{s}]_{\bar{3}_c}]_{\mathbf{1}}$ and $[[cs]_{\bar{6}_c}[\bar{c}\bar{s}]_{\bar{6}_c}]_{\mathbf{1}}$, which are respectively denoted by $\bar{\mathbf{3}}_c - \mathbf{3}_c$ and $\bar{\mathbf{6}}_c - \bar{\mathbf{6}}_c$, can be arrived at and are given in Table III. In the same way, the average distances $\langle \mathbf{r}_{ij}^2 \rangle^{\frac{1}{2}}$ between any two particles and $\langle \mathbf{X}^2 \rangle^{\frac{1}{2}}$ between the diquark $[cs]$ and antiquark $[\bar{c}\bar{s}]$ can also be calculated and are shown in Table IV.

The $\langle \mathbf{r}_{12}^2 \rangle^{\frac{1}{2}}$ and $\langle \mathbf{r}_{34}^2 \rangle^{\frac{1}{2}}$ respectively represent the size of the diquark $[cs]$ and antiquark $[\bar{c}\bar{s}]$. It can be found from Table IV that they share the same value, around 0.6 fm, and are mainly determined by their own inner interactions. They are almost independent of the orbital excitation L and are slightly influenced by the total spin S . The $\langle \mathbf{X}^2 \rangle^{\frac{1}{2}}$ stands for the average distance between the diquark $[cs]$ and antiquark $[\bar{c}\bar{s}]$, which greatly increases with the increase of the orbital excitation L . In the ground states, the short distance $\langle \mathbf{X}^2 \rangle^{\frac{1}{2}}$ ranging from 0.35 to 0.41 fm is less than the size of the diquark $[cs]$ and antiquark $[\bar{c}\bar{s}]$, which indicates that the overlap of the two subclusters is

TABLE III. The mass spectra of the state $[cs][\bar{c}\bar{s}]$ with J^{PC} in the multiquark color flux-tube model; C.C. represents the coupling results of the color configurations $\bar{\mathbf{3}}_c - \mathbf{3}_c$ and $\bar{\mathbf{6}}_c - \bar{\mathbf{6}}_c$, units in MeV.

S	J^{PC}	$L = 0$			$L = 1$			$L = 2$				
		$\bar{\mathbf{3}}_c - \mathbf{3}_c$	$\bar{\mathbf{6}}_c - \bar{\mathbf{6}}_c$	C.C.	J^{PC}	$\bar{\mathbf{3}}_c - \mathbf{3}_c$	$\bar{\mathbf{6}}_c - \bar{\mathbf{6}}_c$	C.C.	J^{PC}	$\bar{\mathbf{3}}_c - \mathbf{3}_c$	$\bar{\mathbf{6}}_c - \bar{\mathbf{6}}_c$	C.C.
0	0^{++}	4360, 39.5%	4318, 60.5%	4239	1^{--}	4629, 95.2%	4802, 4.8%	4620	2^{++}	4868, 99.1%	5163, 0.9%	4865
1	1^{++}	4378, 64.1%	4416, 35.9%	4330	0^{--}	4665, 97.4%	4875, 2.6%	4659	1^{++}	4899, 99.1%	5188, 0.9%	4897
					1^{--}	4664, 97.3%	4872, 2.7%	4659	2^{++}	4900, 99.1%	5188, 0.9%	4897
					2^{--}	4663, 97.3%	4867, 2.7%	4657	3^{++}	4902, 99.1%	5189, 0.9%	4899
1	1^{+-}	4420, 19.0%	4360, 81.0%	4342	0^{+-}	4687, 99.4%	4879, 0.6%	4686	1^{+-}	4925, 99.7%	5164, 0.3%	4924
					1^{+-}	4687, 99.4%	4877, 0.6%	4686	2^{+-}	4926, 99.7%	5165, 0.3%	4925
					2^{+-}	4687, 99.4%	4873, 0.6%	4686	3^{+-}	4928, 99.7%	5166, 0.3%	4927
2	2^{++}	4430, 75.8%	4455, 24.2%	4418	0^{++}	4935, 99.6%	5190, 0.4%	4934	0^{++}	4935, 99.6%	5190, 0.4%	4934
					1^{--}	4705, 99.2%	4911, 0.8%	4704	1^{++}	4935, 99.6%	5190, 0.4%	4934
					2^{--}	4705, 99.2%	4908, 0.8%	4704	2^{++}	4936, 99.6%	5191, 0.4%	4935
					3^{--}	4705, 99.2%	4903, 0.8%	4703	3^{++}	4938, 99.6%	5193, 0.4%	4937
									4^{++}	4940, 99.6%	5194, 0.4%	4939

TABLE IV. The average distances $\langle r_{ij}^2 \rangle^{\frac{1}{2}}$ and $\langle \mathbf{X}^2 \rangle^{\frac{1}{2}}$, units in femtometers.

$S \oplus L$ J^{PC}	$0 \oplus 0$ 0^{++}	$0 \oplus 1$ 1^{--}	$0 \oplus 2$ 2^{++}	$1 \oplus 0$ 1^{++}	$1 \oplus 1$ $0, 1, 2^{--}$	$1 \oplus 2$ $1, 2, 3^{++}$	$1 \oplus 0$ 1^{+-}	$1 \oplus 1$ $0, 1, 2^{+-}$	$1 \oplus 2$ $1, 2, 3^{+-}$	$2 \oplus 0$ 2^{++}	$2 \oplus 1$ $1, 2, 3^{--}$	$2 \oplus 2$ $0, 1, 2, 3, 4^{++}$
$\langle r_{12}^2 \rangle^{\frac{1}{2}}$	0.58	0.59	0.60	0.59	0.60	0.61	0.61	0.61	0.62	0.61	0.61	0.62
$\langle r_{34}^2 \rangle^{\frac{1}{2}}$	0.58	0.59	0.60	0.59	0.60	0.61	0.61	0.61	0.62	0.61	0.61	0.62
$\langle r_{13}^2 \rangle^{\frac{1}{2}}$	0.40	0.63	0.79	0.43	0.64	0.79	0.40	0.64	0.79	0.45	0.65	0.80
$\langle r_{24}^2 \rangle^{\frac{1}{2}}$	0.72	0.88	1.00	0.75	0.89	1.01	0.75	0.90	1.02	0.78	0.91	1.03
$\langle r_{14}^2 \rangle^{\frac{1}{2}}$	0.58	0.77	0.90	0.61	0.78	0.91	0.60	0.78	0.91	0.64	0.79	0.92
$\langle r_{23}^2 \rangle^{\frac{1}{2}}$	0.58	0.77	0.90	0.61	0.78	0.91	0.60	0.78	0.91	0.64	0.79	0.92
$\langle \mathbf{X}^2 \rangle^{\frac{1}{2}}$	0.35	0.60	0.76	0.38	0.61	0.76	0.36	0.61	0.76	0.41	0.62	0.77

extremely strong so that the picture of the diquark and antiquark is not clear. In the excited states, the picture is gradually clear because the diquark $[cs]$ and the antiquark $[\bar{c}\bar{s}]$ are well separated with the increase of the orbital excitation L . The diagrammatic sketch of this picture is shown in Fig. 2.

One can judge from the average distance in Table IV that the diquark $[cs]$ and antiquark $[\bar{c}\bar{s}]$ are not located on a plane but twist into a three-dimensional spatial configuration, which is determined by the dynamics of the systems. First, the configuration of the diquark $[cs]$ and antiquark $[\bar{c}\bar{s}]$ is mainly determined by their inner dynamics. Under the condition of the specified L , the distance between the two subclusters is mainly determined by the competition between their relative motion and the confinement between the two subclusters because the former is inversely proportional to the distance while the latter is proportional to the distance. Second, the other interactions between the two subclusters result in the twist to arrive at a balance so that the diquark and antiquark are not on a plane. The appearance of the tetraquark state $[cs][\bar{c}\bar{s}]$ like a dumbbell; the larger the orbital excitation L , the more distinguished the shape (see Fig. 2). The multibody confinement potential, which is a collective degree of freedom, based on the color flux-tube picture, is the mainly dynamical mechanism of the formation of the picture. Lattice QCD calculation on the tetraquark states indicated that the three-dimensional spatial configuration is more stable than a planar one against transition into mesons [38].

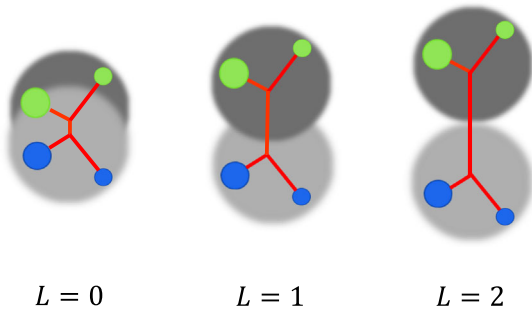


FIG. 2. Diquark-antiquark picture.

To understand dynamical behavior of various interactions in the tetraquark states $[cs][\bar{c}\bar{s}]$, we give the contributions from various parts of the Hamiltonian and the average distances $\langle r_{ij}^2 \rangle^{\frac{1}{2}}$ and $\langle \mathbf{X}^2 \rangle^{\frac{1}{2}}$ in the ground states and $S = 0$ excited states, which are shown in Table V. E_k , V_{\min}^c , V^{cm} , and V^{clb} represent kinetic, confinement potential, color-magnetic interaction, and Coulomb interaction, respectively.

The Coulomb interaction depends on $\frac{1}{r}$ and the color factor $\langle \hat{Q}_{ij} \rangle$ listed in Table VI, which generally provides a very strong attraction; see Table V. The Coulomb interaction is attractive in any two particles in the color configuration $\bar{\mathbf{3}}_c - \mathbf{3}_c$ because of $\langle \hat{Q}_{ij} \rangle < 0$. In the color configuration $\mathbf{6}_c - \bar{\mathbf{6}}_c$, the Coulomb interaction between the diquark $[cs]_{\mathbf{6}}$ and antiquark $[\bar{c}\bar{s}]_{\bar{\mathbf{6}}}$ is attractive and is stronger than that in the color configuration $\bar{\mathbf{3}}_c - \mathbf{3}_c$ because the strength of the interaction depends on the color factor $\langle \hat{Q}_{ij} \rangle$, while the Coulomb interaction within the diquark $[cs]_{\mathbf{6}}$ and antiquark $[\bar{c}\bar{s}]_{\bar{\mathbf{6}}}$ is repulsive because of $\langle \hat{Q}_{12} \rangle = \langle \hat{Q}_{34} \rangle > 0$. Therefore, the final result of the Coulomb interaction in the configuration $\mathbf{6}_c - \bar{\mathbf{6}}_c$ depends on the distance $\langle \mathbf{X}^2 \rangle^{\frac{1}{2}}$ between the diquark $[cs]_{\mathbf{6}}$ and antiquark $[\bar{c}\bar{s}]_{\bar{\mathbf{6}}}$. In the ground states, the distance $\langle \mathbf{X}^2 \rangle^{\frac{1}{2}}$ is small so that the Coulomb interaction between the diquark $[cs]_{\mathbf{6}}$ and antiquark $[\bar{c}\bar{s}]_{\bar{\mathbf{6}}}$ in the color configuration $\mathbf{6}_c - \bar{\mathbf{6}}_c$ is a little stronger than that in the configuration $\bar{\mathbf{3}}_c - \mathbf{3}_c$, which can offset the repulsive interaction in the diquark $[cs]_{\mathbf{6}}$ and antiquark $[\bar{c}\bar{s}]_{\bar{\mathbf{6}}}$. Therefore, the configuration $\mathbf{6}_c - \bar{\mathbf{6}}_c$ cannot be ignored in the ground states because the Coulomb interaction in the color configuration $\mathbf{6}_c - \bar{\mathbf{6}}_c$ is stronger than that in the color configuration $\bar{\mathbf{3}}_c - \mathbf{3}_c$; see Table V. In the excited states, the Coulomb interaction in the color configurations $\mathbf{6}_c - \bar{\mathbf{6}}_c$ and $\bar{\mathbf{3}}_c - \mathbf{3}_c$ rapidly becomes weak because the distance $\langle \mathbf{X}^2 \rangle^{\frac{1}{2}}$ increases with the increase of L . The Coulomb interaction in the color configuration $\bar{\mathbf{3}}_c - \mathbf{3}_c$ is obviously stronger than that in the color configuration $\mathbf{6}_c - \bar{\mathbf{6}}_c$ because of the strong attractive Coulomb interaction in the diquark $[cs]_{\bar{\mathbf{3}}}$ and antiquark $[\bar{c}\bar{s}]_{\mathbf{3}}$. In this way, the

TABLE V. Energy of various parts of the Hamiltonian in MeV and the average distances in femtometers.

LS	J^{PC}	States	Mass, proportion	E_k	V_{\min}^c	V^{cm}	V^{clb}	$\langle r_{12}^2 \rangle^{\frac{1}{2}}$	$\langle r_{34}^2 \rangle^{\frac{1}{2}}$	$\langle r_{13}^2 \rangle^{\frac{1}{2}}$	$\langle r_{24}^2 \rangle^{\frac{1}{2}}$	$\langle r_{14}^2 \rangle^{\frac{1}{2}}$	$\langle r_{23}^2 \rangle^{\frac{1}{2}}$	$\langle X^2 \rangle^{\frac{1}{2}}$
00	0^{++}	$\bar{\mathbf{3}}_c - \mathbf{3}_c$	4360, 39.5%	1061	358	-55	-1271	0.56	0.56	0.47	0.75	0.62	0.62	0.43
		$\mathbf{6}_c - \bar{\mathbf{6}}_c$	4318, 60.5%	1064	322	-104	-1281	0.60	0.60	0.39	0.74	0.59	0.59	0.34
		C.C.	4239	1063	317	-158	-1300	0.58	0.58	0.40	0.72	0.58	0.58	0.35
10	1^{--}	$\bar{\mathbf{3}}_c - \mathbf{3}_c$	4629, 95.2%	1004	423	-53	-1062	0.59	0.59	0.64	0.89	0.77	0.77	0.62
		$\mathbf{6}_c - \bar{\mathbf{6}}_c$	4802, 4.8%	1070	415	-60	-942	0.67	0.67	0.55	0.89	0.74	0.74	0.51
		C.C.	4620	1007	422	-69	-1058	0.59	0.59	0.63	0.88	0.77	0.77	0.60
20	2^{++}	$\bar{\mathbf{3}}_c - \mathbf{3}_c$	4868, 99.1%	1046	520	-51	-965	0.60	0.60	0.79	1.00	0.90	0.90	0.77
		$\mathbf{6}_c - \bar{\mathbf{6}}_c$	5169, 0.9%	1116	507	-30	-747	0.71	0.71	0.70	1.02	0.87	0.87	0.66
		C.C.	4865	1047	520	-55	-965	0.60	0.60	0.79	1.00	0.90	0.90	0.76
01	1^{++}	$\bar{\mathbf{3}}_c - \mathbf{3}_c$	4378, 64.1%	976	330	-22	-1223	0.57	0.57	0.47	0.76	0.63	0.63	0.43
		$\mathbf{6}_c - \bar{\mathbf{6}}_c$	4415, 35.9%	990	351	-1	-1241	0.62	0.62	0.41	0.77	0.61	0.61	0.35
		C.C.	4330	981	337	-50	-1256	0.59	0.59	0.43	0.75	0.61	0.61	0.38
01	1^{+-}	$\bar{\mathbf{3}}_c - \mathbf{3}_c$	4420, 19.0%	954	343	-1	-1194	0.58	0.58	0.47	0.76	0.63	0.63	0.43
		$\mathbf{6}_c - \bar{\mathbf{6}}_c$	4360, 81.0%	983	347	-53	-1234	0.61	0.61	0.40	0.75	0.60	0.60	0.35
		C.C.	4342	977	346	-48	-1251	0.61	0.61	0.40	0.75	0.60	0.60	0.36
02	2^{++}	$\bar{\mathbf{3}}_c - \mathbf{3}_c$	4430, 75.8%	901	354	32	-1175	0.59	0.59	0.48	0.78	0.65	0.65	0.44
		$\mathbf{6}_c - \bar{\mathbf{6}}_c$	4455, 24.2%	926	377	37	-1202	0.63	0.63	0.42	0.78	0.62	0.62	0.36
		C.C.	4418	908	360	38	-1204	0.61	0.61	0.45	0.78	0.64	0.64	0.41

proportion of the color configuration $\mathbf{6}_c - \bar{\mathbf{6}}_c$ is not small or even very big in the ground state. However, the color configuration $\mathbf{6}_c - \bar{\mathbf{6}}_c$ is very small in the excited states while the configuration $\bar{\mathbf{3}}_c - \mathbf{3}_c$ is dominant. The proportion of each color configuration is mainly determined by the Coulomb interaction.

The difference of the Coulomb interaction between the color configurations $\bar{\mathbf{3}}_c - \mathbf{3}_c$ and $\mathbf{6}_c - \bar{\mathbf{6}}_c$ in the ground states is not as obvious as in the excited states because of the small distance $\langle X^2 \rangle^{\frac{1}{2}}$. It can be found from Table V that the mass difference between the color configurations $\bar{\mathbf{3}}_c - \mathbf{3}_c$ and $\mathbf{6}_c - \bar{\mathbf{6}}_c$ in the ground states 0^{++} and 1^{+-} mainly results from the color-magnetic interaction V^{cm} . The color configuration $\mathbf{6}_c - \bar{\mathbf{6}}_c$ is dominant because its V^{cm} is obviously lower than that of the configuration $\bar{\mathbf{3}}_c - \mathbf{3}_c$. For the ground states with 1^{++} and 2^{++} , the difference of V^{cm} between the two color configurations is not obvious, although V^{cm} of the color configuration $\bar{\mathbf{3}}_c - \mathbf{3}_c$ is lower, especially the state 2^{++} . However, E_k and V_{\min}^c of the color configuration $\bar{\mathbf{3}}_c - \mathbf{3}_c$ are both lower than those of the color configuration $\mathbf{6}_c - \bar{\mathbf{6}}_c$. In this way, the masses of the two states with the color configuration $\bar{\mathbf{3}}_c - \mathbf{3}_c$ are lower so that the color configuration $\bar{\mathbf{3}}_c - \mathbf{3}_c$ is dominant.

The color-magnetic interaction is a significant factor resulting in the mass splitting in the states with the same

orbital excitation L but different spin structures. For the ground states, the mass splitting between two adjacent states is about 90 MeV; see the states with 0^{++} , 1^{++} , and 2^{++} in Table III, which is very close to the difference of the corresponding V^{cm} in Table V. For the excited states with orbital excitations $L = 1$ and $L = 2$, the mass splittings are, respectively, around 40 and 35 MeV; see the states 1^{--} and 2^{++} in Table III. The phenomenon of the stable mass difference between two adjacent states can be understood from the spatial distance shown in Table IV, which is mainly determined by the orbital excitation L but slightly influenced by the total spin S . The states with the total spin $S = 1$ and opposite C parity due to different spin-coupling models have close masses. The difference in the ground states is 12 MeV, while the difference in excited states is less than 30 MeV.

The orbital excitation has a great influence on the mass of the state $[cs][\bar{c}\bar{s}]$. It induces a large mass splitting, about several hundred MeVs, among the states with different orbital angular momentum, which mainly comes from the Coulomb interaction and confinement potential; see Table V. The spin-orbit interaction is extremely weak, which brings about a very small mass splitting, less than 5 MeV. Therefore, the masses of the excited states with the same L and S but different total angular momentum J are almost degenerate, which is qualitatively consistent with the conclusion of the work [35]. In addition, the tensor interactions are usually weak as the spin-orbit interaction [39], which is therefore frequently ignored in the preliminary research and should be taken into account in the further investigation of hyperfine structure.

The LHCb Collaboration recently confirmed the states $X(4140)$ and $X(4274)$ in the $J/\Psi\phi$ invariant mass

TABLE VI. Color matrix elements, $\hat{Q}_{ij} = \lambda_i^c \cdot \lambda_j^c$.

$\langle \hat{Q}_{ij} \rangle$	$\langle \hat{Q}_{12} \rangle$	$\langle \hat{Q}_{34} \rangle$	$\langle \hat{Q}_{13} \rangle$	$\langle \hat{Q}_{24} \rangle$	$\langle \hat{Q}_{14} \rangle$	$\langle \hat{Q}_{23} \rangle$
$\langle \bar{\mathbf{3}}_c - \mathbf{3}_c \hat{Q}_{ij} \bar{\mathbf{3}}_c - \mathbf{3}_c \rangle$	$-\frac{8}{3}$	$-\frac{8}{3}$	$-\frac{4}{3}$	$-\frac{4}{3}$	$-\frac{4}{3}$	$-\frac{4}{3}$
$\langle \mathbf{6}_c - \bar{\mathbf{6}}_c \hat{Q}_{ij} \mathbf{6}_c - \bar{\mathbf{6}}_c \rangle$	$\frac{4}{3}$	$\frac{4}{3}$	$-\frac{10}{3}$	$-\frac{10}{3}$	$-\frac{10}{3}$	$-\frac{10}{3}$

distribution and determined their spin-parity quantum numbers to be both 1^{++} [40], which has a large impact on its possible interpretations. The possibility of describing the state $X(4140)$ as a 0^{++} or 2^{++} $D_s^{*+}D_s^{*-}$ molecule state was excluded [41]. At the same time, the depiction of the state $X(4274)$ as a molecular bound state or a cusp cannot account for its quantum numbers [40]. In the present work, the lowest energy of the state $[cs][\bar{c}\bar{s}]$ with 1^{++} is 4330 MeV, see Table III, which is much higher, about 200 MeV, than the state $X(4140)$. In this way, it is difficult to accommodate the state $X(4140)$ as a state $[cs][\bar{c}\bar{s}]$ with 1^{++} in the multiquark color flux-tube model. However, the lowest energy is quite close to the mass of the state $X(4274)$, which implies a possibility that the main component of the state $X(4274)$ may be the state $[cs][\bar{c}\bar{s}]$ with 1^{++} . Many of the previous investigations on the two states also indicated that it is not easy to simultaneously arrange the two states within the same theoretical framework under the assumption of 1^{++} [15,16,42]. However, QCD sum rules and simple color-magnetic interaction models both can interpret the states $X(4140)$ and $X(4274)$ as S -wave states with 1^{++} [8–10].

Accompany with the states $X(4140)$ and $X(4274)$, the high $J/\Psi\phi$ mass region was investigated for the first time with good sensitivity and shows very significant structures, the states $X(4500)$ and $X(4700)$, which can be described as two 0^{++} resonances [40,43]. Comparing the data, the mass of the lowest S -wave $[cs][\bar{c}\bar{s}]$ state with 0^{++} in the present work seems to be too light. It is therefore necessary to introduce radial excitation, D -wave or two P -wave angular excitation, which can satisfy the requirement of quantum numbers. The mass of the lowest D -wave $[cs][\bar{c}\bar{s}]$ state with 0^{++} in Table III is much higher, more than 200 MeV, than those of the states $X(4500)$ and $X(4700)$. Two P -wave excited states are higher than D -wave one. The two states should therefore not be the D -wave or two P -wave angular excited state $[cs][\bar{c}\bar{s}]$ in the present work. The masses of the fourth and fifth S -wave radial excited states $[cs][\bar{c}\bar{s}]$ are respectively 4466 and 4699 MeV, which can match with those of the states $X(4500)$ and $X(4700)$. Zhu also explained the two states as the radial excitation of $J^P = 0^+$ tetraquark state [44]. Chen *et al.* interpreted the two states as the D -wave $[cs][\bar{c}\bar{s}]$ tetraquark states of $J^P = 0^+$ within the framework of QCD sum rules [11]. In addition to the $[cs][\bar{c}\bar{s}]$ explanation, the states $X(4500)$ and $X(4700)$ were described as conventional charmonium states with 4^3P_1 and 5^3P_1 , respectively, in the nonrelativistic constituent quark model [45].

The Belle Collaboration observed a narrow $J/\Psi\phi$ peak at $4350.6_{-5.1}^{+4.6} \pm 0.7$ MeV in two-photon collisions, which implies $J^{PC} = 0^{++}$ or 2^{++} [46]. It is expected that the related experiments can provide more accurate information on the quantum numbers of the state in the future. If $J^{PC} = 0^{++}$, one can find from Table III that the pure $[[cs]_{\bar{3}_c}[\bar{c}\bar{s}]_{\bar{3}_c}]_1$ state with 0^{++} has a mass of 4360 MeV,

which is completely consistent with the experimental data. If $J^{PC} = 2^{++}$, our prediction, 4418 MeV, is a little higher than the result reported by the experiment. Anyway, the state seems to be accommodated in the multiquark color flux-tube model just from the judgement of the mass and quantum number. In the simple color-magnetic interaction model, the states can be assigned as the state $[cs][\bar{c}\bar{s}]$ with 0^{++} [9]. However, the state cannot be interpreted as the $[cs][\bar{c}\bar{s}]$ tetraquark with either 0^{++} and 2^{++} in the QCD sum rules [12].

The states $Y(4626)$, $Y(4630)$, and $Y(4660)$ with 1^{--} were observed by Belle Collaboration in the different processes [2–4]. However, their masses and widths are consistent with each other within errors. Various theoretical explanations of the $Y(4660)$ and $Y(4630)$ have been done to describe their internal structure, in which the two states were interpreted as the same state [47]: the tetraquark state $[cq][\bar{c}\bar{q}]$ and $f_0(980)\psi'$ bound state. In the present work, the P -wave tetraquark state $[cs]^0[\bar{c}\bar{s}]^1 + [cs]^1[\bar{c}\bar{s}]^0$ with 1^{--} has a mass of 4659 MeV, which is consistent with that of the state $Y(4660)$. The P -wave state $[cs]^0[cs]^0$ with 1^{--} has a mass of 4620 MeV, which is compatible with that of the states $Y(4630)$ and $Y(4626)$. In this way, the states $Y(4626)$, $Y(4630)$, and $Y(4660)$ can be uniformly described as the P -wave tetraquark state $[cs][\bar{c}\bar{s}]$ with 1^{--} . The states $Y(4630)$ and $Y(4626)$ have the same spin structure, which consists of a scalar $[cs]$ and a scalar $[\bar{c}\bar{s}]$, so that they are the same state in the present work. However, the state $Y(4660)$ is made of a scalar $[cs]$ ($[\bar{c}\bar{s}]$) and an axial-vector $[\bar{c}\bar{s}]$ ($[cs]$), which is supported by the result of QCD sum rules [7]. The color configuration $[[cs]_{\bar{3}_c}[\bar{c}\bar{s}]_{\bar{3}_c}]_1$ in the three states is an overwhelming advantage, or the color configuration $[[cs]_{6_c}[\bar{c}\bar{s}]_{\bar{6}_c}]_1$ can be ignored.

The P -wave state $[cs]^1[cs]^1$ with 1^{--} has a mass of 4704 MeV, which is not far from that of the state $Y(4660)$. As a matter of fact, the three states $[cs][\bar{c}\bar{s}]$ with 1^{--} predicted by the model can intermix through the tension interaction, which is left for precision calculation in the future. It can be anticipated that the tension interaction should be weak and does not change the present qualitative conclusion. The interpretations provide new insights into the inner structure of the states $Y(4626)$, $Y(4630)$, and $Y(4660)$ from the perspective of the phenomenological model. What the real structures of the three states are, which needs more experiments and theoretical work to analyze their properties in the future. As a byproduct, the masses of the P -wave states $[bs][\bar{b}\bar{s}]$ with 1^{--} are estimated in the multiquark color flux-tube model, which are in the range of 11,099 to 11,134 MeV. We propose to search for them in the $\Upsilon\phi$ invariant mass distribution in the future.

The assignment of the $[cs][\bar{c}\bar{s}]$ component of the states discussed in the present work is completed just based on the proximity to the experimental masses. The more rigorous test of the component of these states is to study their decay

behavior. The states should eventually decay into several color-singlet mesons due to their high energy. In the course of the decay, the three-dimensional spatial structure must collapse first because of the breakdown of the color flux tubes, and then the decay products form by means of the recombination of color flux tubes. The decay widths are determined by the transition probability of the breakdown and recombination of color flux tubes, which is worthy of further research in the future work.

V. CONCLUSIONS

We systematically study the state $[cs][\bar{c}\bar{s}]$ with the diquark-antidiquark picture in the multi-quark color flux-tube model with a multibody confinement potential and one-gluon-exchange interaction. The sizes of the diquark $[cs]$ and antidiquark $[\bar{c}\bar{s}]$ share the same value, which is almost independent of the orbital excitation L and is slightly influenced by the total spin S . The average distance between the diquark $[cs]$ and antidiquark $[\bar{c}\bar{s}]$ greatly increases with the increase of the orbital excitation L . The appearance of the tetraquark state $[cs][\bar{c}\bar{s}]$ is therefore like a dumbbell; the larger the orbital excitation L , the more distinguished the shape. The multibody confinement potential is the mainly dynamical mechanism of the formation of the picture. The mixing of the two color configurations $[[cs]_{\bar{3}_c}[\bar{c}\bar{s}]_{\bar{3}_c}]_1$ and $[[cs]_{\bar{6}_c}[\bar{c}\bar{s}]_{\bar{6}_c}]_1$ in the ground states is strong, while the color configuration $[[cs]_{\bar{3}_c}[\bar{c}\bar{s}]_{\bar{3}_c}]_1$ is favored and absolutely predominant in the excited states.

The states $Y(4626)$, $Y(4630)$, and $Y(4660)$ can be uniformly described as the P -wave tetraquark state $[cs][\bar{c}\bar{s}]$ with 1^{--} in the multi-quark color flux-tube model. The states $Y(4626)$ and $Y(4630)$ can be interpreted as the same state consisting of a scalar $[cs]$ and a scalar $[\bar{c}\bar{s}]$, while

the state $Y(4660)$ is made of a scalar $[cs]$ ($[\bar{c}\bar{s}]$) and an axial-vector $[\bar{c}\bar{s}]$ ($[cs]$). Their hidden bottom partner has a mass in the range of 11,099 to 11,134 MeV and can be searched for in the $\Upsilon\phi$ invariant mass distribution in the future. The properties of the states $X(4140)$, $X(4274)$, $X(4350)$, $X(4500)$, and $X(4700)$ are also discussed in the model. The state $X(4274)$ is quite close to the lowest mass of the state $[cs][\bar{c}\bar{s}]$ with 1^{++} . The states $X(4500)$ and $X(4700)$ can be described as the fourth and fifth excited states of the ground state $[cs][\bar{c}\bar{s}]$ with 0^{++} . The masses of the ground states $[cs][\bar{c}\bar{s}]$ with 0^{++} and 2^{++} are both close to that of the state $X(4350)$. However, the lightest state $X(4140)$ regarded as the state $[cs][\bar{c}\bar{s}]$ with 1^{++} cannot be accommodated in the model. These results to some extent reinforce the validity of the multi-quark color flux-tube model to quantitatively describe the phenomenology of the multi-quark states and get insights on the dynamics that leads to their formation.

As an outlook of the continuation of this work, the string flip-flop potential regarded as the correct phenomenological model for the confinement should be taken into account. The flip-flop potential is important for the properties of the tetraquark states, especially for the decay process into two mesons.

ACKNOWLEDGMENTS

This research is partly supported by the National Science Foundation of China under Contracts No. 11875226 and No. 11775118; the Natural Science Foundation of Chongqing, China, under Project No. cstc2019jcyj-msxmX0409; and Fundamental Research Funds for the Central Universities under Contract No. SWU118111.

-
- [1] F. K. Guo, C. Hanhart, U.-G. Meißner, Q. Wang, Q. Zhao, and B. S. Zou, *Rev. Mod. Phys.* **90**, 015004 (2018); S. L. Olsen, T. Skwarnicki, and D. Zieminska, *Rev. Mod. Phys.* **90**, 015003 (2018).
 - [2] S. Jia *et al.* (Belle Collaboration), *Phys. Rev. D* **100**, 111103 (2019).
 - [3] X. L. Wang *et al.* (Belle Collaboration), *Phys. Rev. Lett.* **99**, 142002 (2007).
 - [4] G. Pakhlova *et al.* (Belle Collaboration), *Phys. Rev. Lett.* **101**, 172001 (2008).
 - [5] M. Karliner and J. L. Rosner, *Phys. Rev. Lett.* **115**, 122001 (2015).
 - [6] M. Karliner and J. L. Rosner, *Nucl. Phys.* **A954**, 365 (2016).
 - [7] R. M. Albuquerque and M. Nielsen, *Nucl. Phys.* **A815**, 53 (2009).
 - [8] F. Stancu, *J. Phys. G* **37**, 075017 (2010).
 - [9] J. Wu, Y. R. Liu, K. Chen, X. Liu, and S. L. Zhu, *Phys. Rev. D* **94**, 094031 (2016).
 - [10] W. Chen and S. L. Zhu, *Phys. Rev. D* **83**, 034010 (2011).
 - [11] H. X. Chen, E. L. Cui, W. Chen, X. Liu, and S. L. Zhu, *Eur. Phys. J. C* **77**, 160 (2017).
 - [12] W. Chen, H. X. Chen, X. Liu, T. G. Steele, and S. L. Zhu, *Phys. Rev. D* **96**, 114017 (2017).
 - [13] P. G. Ortega, J. Segovia, D. R. Entem, and F. Fernandez, *Phys. Rev. D* **94**, 114018 (2016); Y. F. Yang and J. L. Ping, *Phys. Rev. D* **99**, 094032 (2019).
 - [14] Q. F. Lü and Y. B. Dong, *Phys. Rev. D* **94**, 074007 (2016).
 - [15] R. F. Lebed and A. D. Polosa, *Phys. Rev. D* **93**, 094024 (2016).
 - [16] M. Padmanath, C. B. Lang, and S. Prelovsek, *Phys. Rev. D* **92**, 034501 (2015).
 - [17] Y. Tan and J. L. Ping, [arXiv:1911.02461v1](https://arxiv.org/abs/1911.02461v1); J. He, Y. Liu, J. T. Zhu, and D. Y. Chen, [arXiv:1912.08420v1](https://arxiv.org/abs/1912.08420v1).

- [18] J. L. Ping, C. R. Deng, F. Wang, and T. Goldman, *Phys. Lett. B* **659**, 607 (2008); C. R. Deng, J. L. Ping, Y. C. Yang, and F. Wang, *Phys. Rev. D* **88**, 074007 (2013); C. R. Deng, J. L. Ping, H. X. Huang, and F. Wang, *Phys. Rev. D* **95**, 014031 (2017).
- [19] J. M. Richard, A. Valcarce, and J. Vijande, *Phys. Rev. D* **95**, 054019 (2017); J. Vijande, A. Valcarce, and J. M. Richard, *Phys. Rev. D* **85**, 014019 (2012); **76**, 114013 (2007).
- [20] M. Cardoso, N. Cardoso, and P. Bicudo, *Phys. Rev. D* **86**, 014503 (2012); N. Cardoso and P. Bicudo, *Phys. Rev. D* **87**, 034504 (2013).
- [21] J. Vijande, F. Fernandez, and A. Valcarce, *J. Phys. G* **31**, 481 (2005).
- [22] G. M. Prospero, M. Raciti, and C. Simolo, *Prog. Part. Nucl. Phys.* **58**, 387 (2007).
- [23] J. Weinstein and N. Isgur, *Phys. Rev. D* **27**, 588 (1983).
- [24] J. Weinstein and N. Isgur, *Phys. Rev. Lett.* **48**, 659 (1982).
- [25] J. Weinstein and N. Isgur, *Phys. Rev. D* **41**, 2236 (1990).
- [26] V. Dmitrasinovic, *Phys. Rev. D* **67**, 114007 (2003).
- [27] A. Di Giacomo, M. Maggiore, and S. Olejnik, *Phys. Lett. B* **236**, 199 (1990); V. Singh, D. Browne, and R. Haymaker, *Phys. Lett. B* **306**, 115 (1993); G. S. Bali, C. Schlichter, and K. Schilling, *Phys. Rev. D* **51**, 5165 (1995).
- [28] D. Bugg, *Phys. Rep.* **397**, 257 (2004).
- [29] Y. Nambu, *Phys. Rev. D* **10**, 4262 (1974); G. 't Hooft, *Nucl. Phys. B* **153**, 141 (1979); S. Mandelstam, *Phys. Rep.* **23**, 245 (1976).
- [30] C. Alexandrou, P. de Forcrand, and A. Tsapalis, *Phys. Rev. D* **65**, 054503 (2002); T. T. Takahashi, H. Suganuma, Y. Nemoto, and H. Matsufuru, *Phys. Rev. D* **65**, 114509 (2002); F. Okiharu, H. Suganuma, and T. T. Takahashi, *Phys. Rev. Lett.* **94**, 192001 (2005).
- [31] T. Goldman and S. Yankielowicz, *Phys. Rev. D* **12**, 2910 (1975).
- [32] S. N. Chen and J. L. Ping, *Mod. Phys. Lett. A* **27**, 1250025 (2012).
- [33] J. L. Ping, F. Wang, and T. Goldman, *Nucl. Phys. A* **657**, 95 (1999); A. Valcarce, H. Garcilazo, and F. Fernández, and P. González, *Rep. Prog. Phys.* **68**, 965 (2005).
- [34] G. S. Bali, *Phys. Rev. D* **62**, 114503 (2000); C. Semay, *Eur. Phys. J. A* **22**, 353 (2004); N. Cardoso, M. Cardoso, and P. Bicudo, *Phys. Lett. B* **710**, 343 (2012).
- [35] M. Cleven, F. K. Guo, C. Hanhart, Q. Wang, and Q. Zhao, *Phys. Rev. D* **92**, 014005 (2015).
- [36] F. Okiharu, H. Suganuma, and T. T. Takahashi, *Phys. Rev. D* **72**, 014505 (2005); P. Bicudo and M. Cardoso, *Phys. Rev. D* **83**, 094010 (2011).
- [37] E. Hiyama, Y. Kino, and M. Kamimura, *Prog. Part. Nucl. Phys.* **51**, 223 (2003).
- [38] F. Okiharu, H. Suganuma, and T. T. Takahashi, *Phys. Rev. D* **72**, 014505 (2005).
- [39] M. Furuichi, K. Shimizu, and S. Takeuchi, *Phys. Rev. C* **68**, 034001 (2003).
- [40] R. Aaij *et al.* (LHCb Collaboration), *Phys. Rev. Lett.* **118**, 022003 (2017).
- [41] X. Liu and S. L. Zhu, *Phys. Rev. D* **80**, 017502 (2009); T. Branz, T. Gutsche, and V. E. Lyubovitskij, *Phys. Rev. D* **80**, 054019 (2009); R. M. Albuquerque, M. E. Bracco, and M. Nielsen, *Phys. Lett. B* **678**, 186 (2009).
- [42] V. V. Anisovich, M. A. Matveev, A. V. Sarantsev, and A. N. Semenova, *Int. J. Mod. Phys. A* **30**, 1550186 (2015).
- [43] R. Aaij *et al.* (LHCb Collaboration), *Phys. Rev. D* **95**, 012002 (2017).
- [44] R. L. Zhu, *Phys. Rev. D* **94**, 054009 (2016).
- [45] P. G. Ortega, J. Segovia, D. R. Entem, and F. Fernández, *Phys. Rev. D* **94**, 114018 (2016).
- [46] C. P. Shen *et al.* (Belle Collaboration), *Phys. Rev. Lett.* **104**, 112004 (2010).
- [47] D. V. Bugg, *J. Phys. G* **36**, 075002 (2009); G. Cotugno, R. Faccini, A. D. Polosa, and C. Sabelli, *Phys. Rev. Lett.* **104**, 132005 (2010); F. K. Guo, J. Haidenbauer, C. Hanhart, and U. G. Meissner, *Phys. Rev. D* **82**, 094008 (2010).